NUMERICAL EXPERIMENTS INVESTIGATING THE SOURCE OF EXPLOSION S-WAVES

Stephen C. Myers, Jeffery L. Wagoner, and Shawn C. Larsen

Lawrence Livermore National Laboratory

Sponsored by National Nuclear Security Administration
Office of Nonproliferation Research and Development
Office of Defense Nuclear Nonproliferation

Contract No. W-7405-ENG-48/ROA02-08

ABSTRACT

In this study we use validated explosion simulations to investigate the locations at which explosion S-waves originate. Several mechanisms for generating S-waves from an explosion source have been put forward. These mechanisms include tectonic release, non-symmetrical source effects, non-linear source effects, conversion of P-waves to S-waves off the free surface, and scattering of near-source Rayleigh waves. Each of these mechanisms is physically sound, and each mechanism likely contributes to the observed S-wave field. Identifying where explosion S-waves originate provides an important constraint on the contribution of each S-wave mechanism. The simulations in this study are based on the well-recorded 1993 Nonproliferation experiment (NPE) (chemical kiloton). A regional 3-dimensional model surrounding the NPE is validated by first extracting vertical cross-sections cutting through the NPE source and stations at which the NPE was recorded. We then generate synthetic seismograms using a 2-dimensional finite difference calculation for each event-station path. Good agreement between synthetic and observed seismograms provides confidence that the model and simulations are reasonably accurate. The origin of S-waves is determined through both analysis of the simulated wavefield evolution and using the time-reversal method to refocus far-field S-waves back to their origin. Preliminary results suggest that the primary S-wave pulse originates near the free surface and at high-impedance geologic interfaces that are close to the explosion. These results suggest that scattering can account for much of the observed S-wave energy radiated from the NPE explosion.

OBJECTIVE

Regional monitoring relies heavily on comparisons of P- and S-phase amplitudes (Pomeroy et al., 1982; Walter et al., 1995). Further, widely used methods of determining magnitude make use of Lg and Lg coda amplitudes (e.g., Nuttli, 1986; Mayeda and Walter, 1996; Patton, 2001), and regional S-phases often add important arrival-time observations to limited, small-magnitude datasets used for location (PNE volume, 1994; Mayeda and Walter, 1996; Myers et al., 1999).

Most investigators agree that appreciable energy from the explosions is converted to S-waves near the source, but the dominant P-to-S transfer mechanism is not agreed upon. Several physically reasonable transfer mechanisms are proposed, including P-to-S conversion at the free surface, spall, scattering of short-period surface waves, tectonic release, and rock-damage (e.g., Vogfjord, 1997; Day and Mclaughlin, 1991; Gupta et al., 1992; Wallace et al., 1985; Johnson and Sammis, 2001). Each mechanism fits a subset of observations, and each mechanism, with the exception of surface-wave scattering, is understood from first principles. Currently the Rg-to-S mechanism is represented by an empirical transfer function (e.g., Gupta et al., 1992; Patton, 2001).

Most recent progress of this project has been to use the time-reversal technique with validated numerical simulations to identify the location at which S-waves originate.

RESEARCH ACCOMPLISHED

In previous years of this project we developed a detailed upper-crustal model centered on the 1993 NPE shot (Figure 1). The local model is 20 km on a side (including depth), and construction of the model leverages the extensive Lawrence Livermore National Laboratory (LLNL) database of geological and geophysical information that includes mapping, bore-hole logs, seismic surveys, and gravity surveys (e.g., Healey et al., 1963). While much of LLNL geological database is unpublished, it constitutes a wealth of knowledge that was accumulated over decades of study at the Nevada Test Site (NTS).

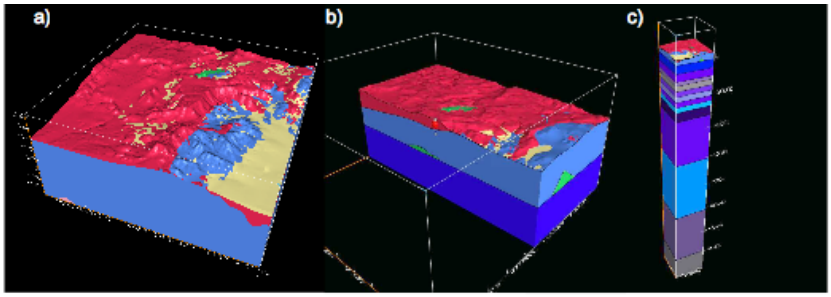

Figure 1. Local model around NPE shot determined from detailed geologic and geophysical studies. a) The entire local model. b) Cross section through the NPE shot. c) Local model merged into a lithospheric velocity stack.

The local model is imbedded in a regional model that extends to ~400km from the NPE source (Figure 2). The default velocity structure is a one-dimensional model based on work of Patton and Taylor (1984). Deviation from the default model is based on published studies in the region. The current version of the model includes variations in upper-crustal structure based on regional geologic maps of Nevada, Utah, California, and Arizona. We assume that crystalline rocks are continuous into the lower crust and that basin depths are proportional to the magnitude of local gravity anomalies (e.g., Blakely et al., 1997). The lower crustal velocities and Moho depth are modified based on the work of Zandt et al. (1994) and Mooney et al. (1998). Minor modifications to mantle velocities are based on refraction profiles summarized in Mooney et al. (1998). In specific areas we have incorporated tomographic studies, such as Biasi (2005) and Preston et al. (2005).

Considerable effort has been put into translating EarthVision models—as seen in Figures 1 and 2—into seismic models. We have developed a suite of codes that translate geologic units into either a constant P-wave, S-wave, and density or into a geologic unit may be translated into a specified portion of a

velocity/depth profile. Generally, the upper crust is modeled as constant velocity units, such as sedimentary units and granite bodies. The lower crust and upper mantle are modeled as smooth velocity vs. depth profiles, which are allowed to change laterally. Modeling the lower crust and upper mantle with smooth velocity profiles, as opposed to discrete layers, eliminates nuisance reflections and conversions from P to S energy.

.

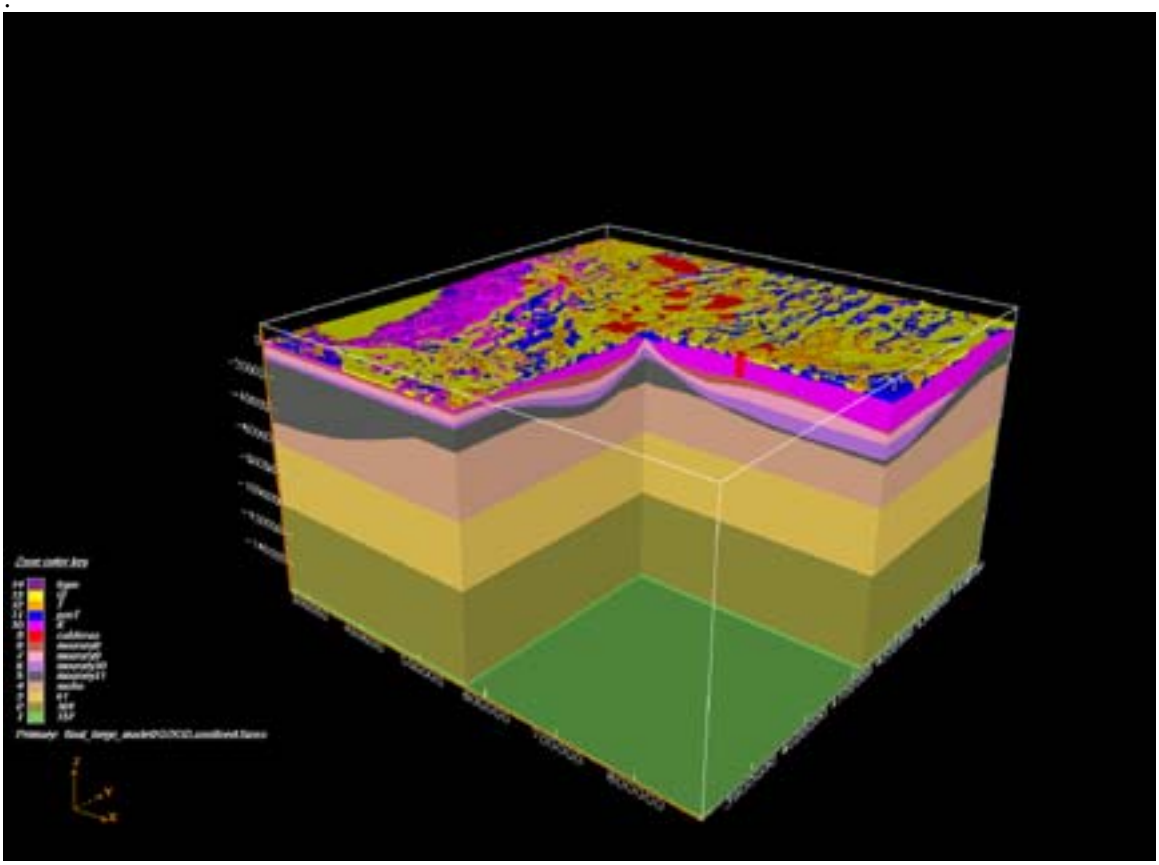

Figure 2. Regional geologic model centered on the Nevada Test Site. The model extends into California (to the left), Utah, and Arizona (to the right). The model is a compilation of geologic mapping; seismic profiles, receiver functions, and tomography; and gravity modeling for basin structure.

Model Validation Using NPE Observations

We use the E3D code of Larson and Grieger (1998) for seismic simulations. E3D is a full elastic code that allows the input of a general geologic structure, including the free surface. All of our simulations use a grid spacing of 60 meters, which enables interpretation to 3 or 4 Hz.

Our numerical simulations are based on the 1993 NPE. The NPE was a 1-kiloton chemical explosion at the NTS. NPE details and research reports can be found in Denny and Stull (1994). Figure 3 shows the extensive network of stations that recorded the NPE. We have compiled all these recordings to validate our model. We begin with the local recordings, which we used both to validate the near-source model and to estimate the NPE moment tensor.

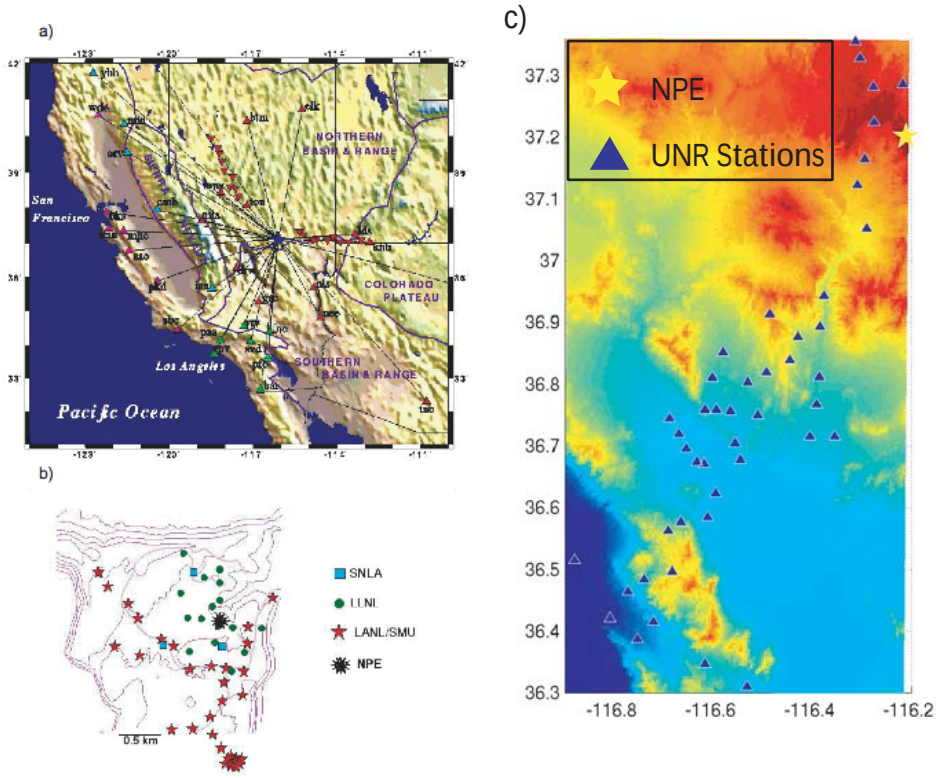

Figure 3: Stations with recordings of the NPE shot. We have compiled waveforms from all of these stations.

Figure 4 shows an example waveform (black) from a station that is approximately 2 km from the NPE. Simulations (red) with combinations of isotropic (Figure 4 a,b) and compensated linear vector dipoles (CLVD) (Figure 4 c,d) moment tensors and topographic free surface (Figure 4 a,c) and flat free surface (Figure 4 b,d) are compared with the data. It is clear that the isotropic source in a model that includes the topographic free surface is the best fit to the data. Comparisons with other local data (not shown) are similar, and we conclude that the NPE is best modeled as an isotropic source.

Figure 5 is an example of our regional validation effort. In this example we use the temporary, broadband (STS-2 sensor) deployment fielded by the University of Arizona. The cross section is color coded to P-wave velocity, which was taken from our regional 3-dimensional model. The upper crust is characterized by Paleozoic sedimentary rocks, which are interrupted by low-velocity basins. Velocity in the mid- and lower crust primarily increases with depth, but we include minor lateral variation in velocity as well has changes in Moho depth based on the work of Zandt et al. (1995). The interface between light and dark red in the lower quarter of the cross section is the Moho. We have superimposed a snapshot of the seismic wavefield on the cross section to demonstrate the complexity that results from this relatively simple model.

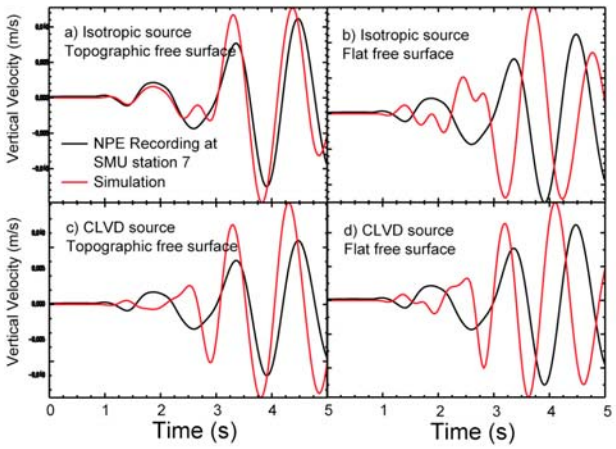

Figure 4. Recorded (black) and simulated (red) displacement seismograms for the NPE shot. These 3-dimensional simulations make use of the local NPE model (see above). Event-station distance is approximately 2 km. The NPE is best modeled as an isotropic source. Simulation with a realistic free surface is essential to match the data.
a) Simulation with isotropic moment tensor and free surface based on digital elevation model digital elevation model (DEM).
b) Simulation with isotropic source and flat free surface.
c) Simulation with CLVD moment tensor with DEM free surface.
d) Simulation with CLVD moment tensor and flat free surface.

The traces shown in Figure 5 compare recorded (black) and synthetic (red) velocity seismograms. Both velocity and synthetic records are band passed between 0.7 Hz and 3 Hz. Amplitudes are normalized because geometric spreading in the 2-dimensional synthetics is incorrect. In general, the comparison of observed and synthetic data is favorable. The degree of waveform complexity is nearly identical, and it would be difficult to tell which trace is real based on simple inspection. The relative amplitudes of the real and synthetic waveforms are also in good agreement (with the notable exception of station 8, where synthetic amplitudes after the first arrival are too large). Although the phase is matched in many instances (particularly the first arrival), we cannot claim to have simulated phase reliably. Nonetheless, the overall agreement between observed and synthetic data is very good, especially considering that the model was not directly derived from the data. Figure 5b shows cumulative energy for the 6 recordings and synthetics. In most cases the cumulative energy curves of data and synthetics are in good agreement. We also note that synthetic estimates are high in some case and low in others. i.e., there is not a consistent bias across all stations. We find that the overall model performance is good and that variability can be attributed to station site effects.

Observed and synthetic P/S ratios are in good (but not perfect) agreement (Table 1; Figure 6). In a band-pass of 0.5 Hz to 1.0 Hz the data are biased towards higher P/S ratios. We are currently working to understand the bias, but we note that the bias is only a couple tenths, which is well within the spread of most empirical P/S plots. In the 1.0 Hz to 3.0 Hz band P/S ratios for both data and synthetics increase, suggesting that our model is characterizing the wavefield at these frequencies.

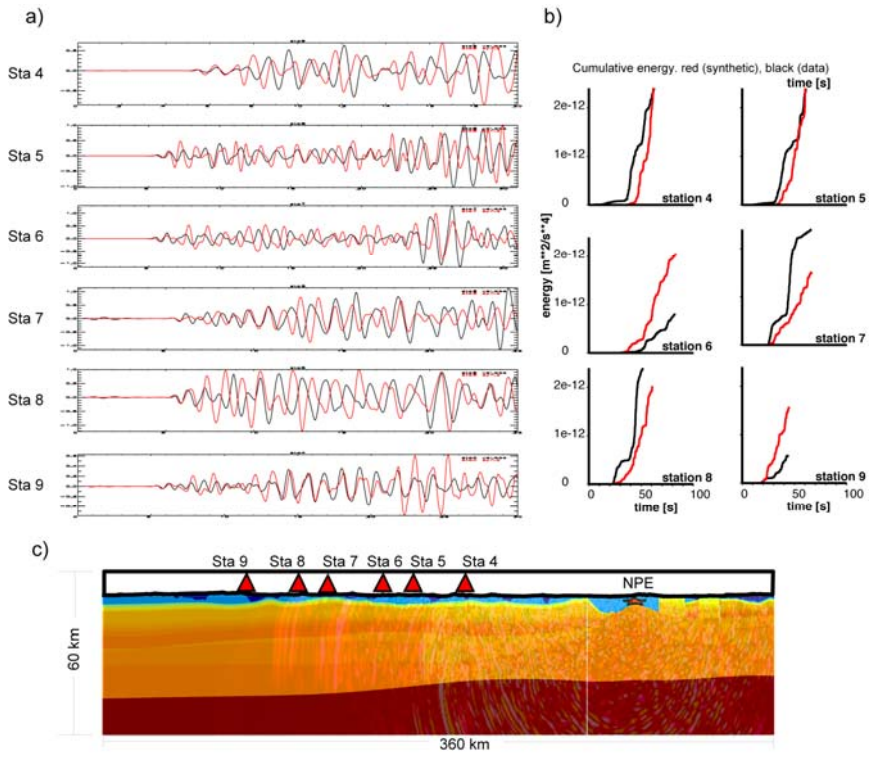

Figure 5. Model validation with regional seismic simulations of the University of Arizona broadband deployment (line extending east from NPE in Figure 2). a) Vertical velocity recordings of the NPE between 0.7 Hz and 3 Hz (black) with synthetics (red) for comparison. Amplitudes are normalized. A separate 2-dimensional simulation was made for each of the stations to account for slight azimuth variations in structure. The general character of the observed seismograms is matched by the synthetics, suggesting that the regional model is a good representation of true structure. b) Cumulative energy for observed and synthetic waveforms in a). c) Cross section shows a snapshot of the seismic wavefield overlain on a P-wave velocity for the station 9 simulation; west is to the right. The transition from red to near black in the lower quarter of the cross section is the Moho.

Table 1: P/S ratio for data and synthetics

	0.5 to 1.0 Hz		1.0 to 3.0 Hz	
	data	synth	data	synth
sta4	0.504	0.143	1.568	0.374
sta5	0.592	0.200	0.551	0.601
sta6	0.153	0.230	0.336	0.424
sta7	0.724	0.518	0.860	1.290
sta8	1.032	0.406	1.665	0.469
sta9	0.741	0.480	0.934	0.802

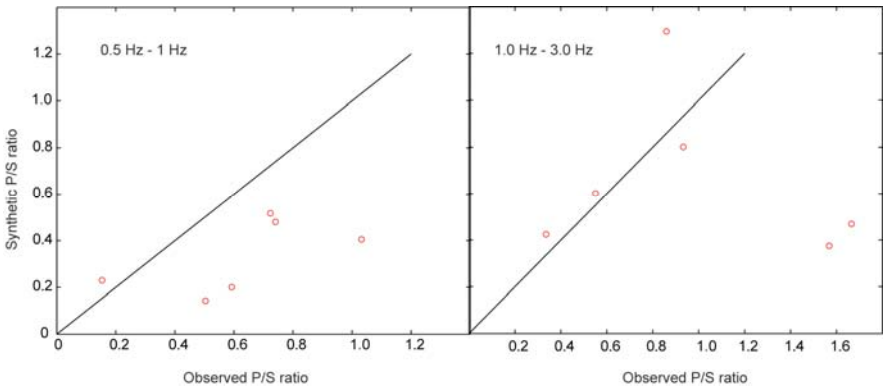

Figure 6. Comparison of observed and synthetic P/S ratios

Time Reversal to Locate S-Wave Origins

Using an isotropic source and our model that is based on geologic compilation, we reproduce the travel-times and first few swings of local and regional body phases. The amplitude characteristics of later portions of the regional phases (after the first swings) are generally in agreement with data, but the simulations are generally not in phase with data. These simulations use the simplest model that includes the known topography and geologic structure and uses the simplest explosion source (isotropic). Agreement between simulations and empirical data suggest that accounting for the known geologic structure can reproduce much of the waveform complexity and S-wave generation that is observed in the data.

Because the simulations use an isotropic source (pure P-wave source), the origin of the S-waves is in question. Visual examination of the wave field evolution over time shows that S-waves originate near the isotropic source, but the exact location(s) remains unclear.

We employ time-reversal techniques to better resolve the S-wave origin(s) (e.g., Larmat et al., 2006). As a first test of this approach we use 2-dimensional simulations (vertical cross-section) oriented approximately east-west through the NPE explosion (similar to Figure 5). The isotropic source is used, and the wave field is recorded at sensors approximately 20 km from the source. The sensors, which are not restricted to the free surface, are positioned at increments of 10° inclination in the vertical plane. Because the source is near the surface, 10° sampling results in 18 sensors. Using the divergence and curl operators on the simulated wave field, we isolate the P- and S-wave portions of the velocity seismograms (Figure 7). We then cut and time-reverse the initial P- and S-wave pulses and formulate the P- and S-wave moment tensors at each sensor. The P- and S-wave, time-reversed simulations are conducted separately to isolate the source of the two types of waves.

Figure 8 shows the results of the P- and S-wave time-reversal experiments. In both Figure 8a and 8b the peak particle velocity is normalized by node-specific material impedance to ascertain a node-by-node measurement of wave energy. In the case of P-wave time reversal (Figure 8a), the peak P-wave energy is—as expected—at the location of the simulated source (the source coincides with the red peak in energy in Figure 8a). Considerable energy in the first 1.5 seconds of the P-wave pulse is also seen to emanate from the free surface directly above the source.

In the case of S-wave time reversal (Figure 8b), the peak S-wave energy is along the sloping free surface to the east (right in Figure 8b) of the isotropic source (the eastern edge of Rainier Mesa). Some S-wave energy also emanates from the small basin to the west of the source. As expected, negligible S-wave energy originates at the isotropic source. We note that large velocity contrasts exist near the source, yet most of the S-wave energy originates at irregularities in the free surface near the source.

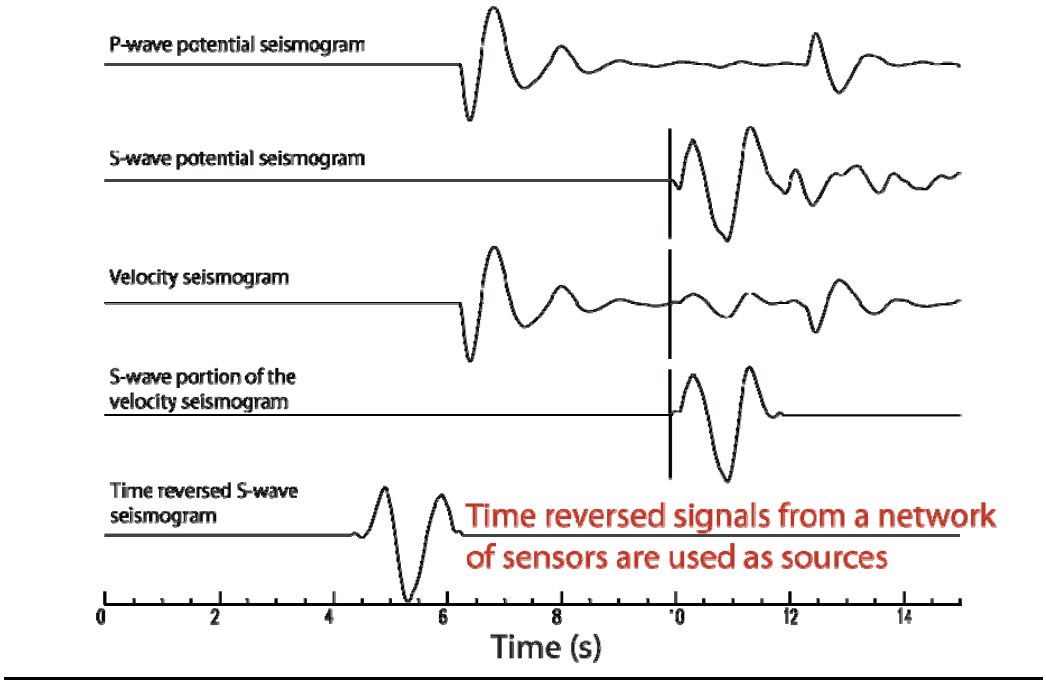

Figure 7. Time reversal procedure. Using the P- and S-potentials, we isolate the S-wave component of the velocity seismogram. We then reverse the S-wave component of the velocity seismogram and use it as a source in a simulation. Using many time-reversed sources we refocus S-wave energy back to its origin.

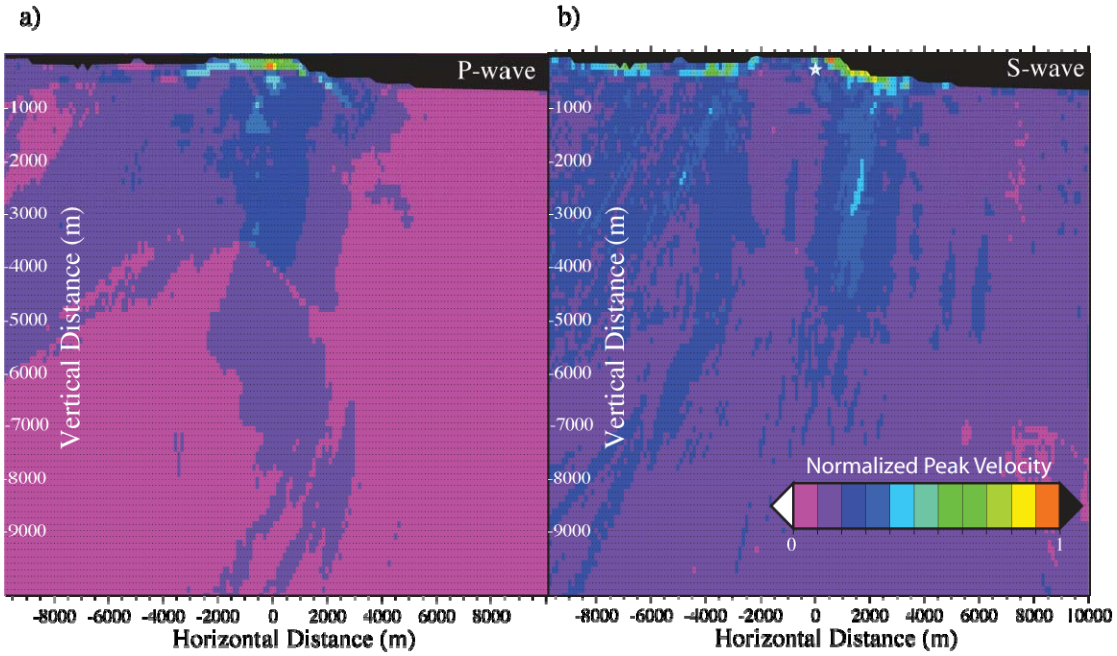

Figure 8. Peak, impedance-normalized velocity for time reversal of first 1.5 seconds of a) P-wave and b) S-waves. Peak(s) occur at the source of the waves. P-waves originate predominantly from the isotropic source and from reflection off the free surface. S-waves originate from the predominantly from the steep gradient in topography near the isotropic source.

CONCLUSIONS AND RECOMMENDATIONS

We have constructed a regional model centered on the NTS based on published and unpublished studies. The starting point of the regional model is a 1-dimensional model that is based on surface-wave studies. We include significant 3-dimensional modifications to the 1-dimensional model based on receiver function, refraction, reflection, and gravity studies. The regional model includes a detailed upper crustal model centered on the NPE explosion. This local model is constrained by geologic maps, borehole data, and geophysical studies at the NTS. The local model is seamlessly embedded into a regional model to enable realistic simulations of NTS sources to regional distance.

Validation of the model is based on recordings and simulations of the NPE shot, as well as phase travel-times from NTS explosions (Sweeney et al., 2006). Validation of the local model is complete and the model reliably predicts local NPE waveforms. Arrival times and relative amplitudes of regional phases are reliably predicted.

Local 3-dimensional simulations demonstrate that topographic scattering is an important source of S-wave generation for the NPE. We find that topographic scattering peaks S-wave amplitudes at approximately 1 Hz, which is in agreement with observations in many instances (at NTS and other locales). Topographic scattering produces a disordered wavefield and scatters energy in all directions. Simulations with a flat free surface produce S-waves, but little frequency dependence is observed.

The agreement between data and simulations is achieved with an isotropic (pure explosion) source. Therefore, we are not compelled to add complexity to the simple explosion source. Although simulated S-waves are qualitatively seen to originate near the isotropic source, the exact origin of the S-waves in these simulations is not entirely clear. We employ a time-reversal technique to better localize the origin of the initial P- and S-wave pulses. We find, as expected, that the initial P-pulse originates from the isotropic source and from the free surface directly above the source. S-waves originate from the steep topographic gradient to the east of the isotropic source (the edge of Rainier Mesa), but not symmetrically above the source, as analytical calculations would suggest.

ACKNOWLEDGEMENTS

We acknowledge the LLNL containment program for generous access to their extensive database of geologic and geophysical studies at the NTS. We also would like to thank Glenn Biasi and Walter Mooney for providing regional geophysical information. This work was also completed in cooperation with the University of Nevada, Reno (UNR), contract DE-FC03-02SF22656, and LLNL benefited from the structural information and tomographic studies conducted at UNR.

REFERENCES

Blakely, R. J., R. C. Jachens, J. P. Calzia, and V. E. Langenheim (1997). Cenozoic basins of the Death Valley extended terrane as reflected in regional-scale gravity anomalies, in Wright, L.A. and B.W. Troxel, eds., Cenozoic Basins of the Death Valley Region: Boudler, CO, *Geol. Soc. Am. Special Paper 333*.

Biasi, G. (2005). Mantle lithospheric clues to Walker Lane evolution, *Presented at the 2005 SSA meeting*, Incline, NV.

Day, S., and K. Mclaughlin (1991). Seismic source representations for spall, *Bull. Seismol. Soc. Am*. 81: 191–201.

Denny, M. D., S .P. Stull (1994). Proceedings of the Symposium on The Non-Proliferation Experiment (NPE): Results and Implications for Test Ban Treaties, Rockville Maryland; Lawrence Livermore National Laboratory.

Gupta, I. N., W. W. Chan, and R. A. Wagner (1992). A comparison of regional phases from underground nuclear explosions at East Kazakh and Nevada Test Sites, *Bull. Seismol. Soc. Am*. 82: 352–382.

Healey, D. L. and Miller, C. H., (1963). Gravity survey of the Gold Meadows Stock, Nevada Test Site, Nye County, Nevada. *USGS Technical Letter NTS-40*.

Johnson, L. R., and C. G. Sammis (2001). Effects of rock damage on seismic waves generated by explosions, *Pageoph*, 158: 1869–1908.

Larmat, C., J-P Montagner, M. Fink, Y Capdeville, A. Tourin, and E. Cevede (2006). Time-reversal imaging of seismic sources and application to the great Sumatra earthquake, *Geophys. Res. Lett*. 33: doi:10.1029/2006GL026336.

Larsen, S., and J. Grieger (1998). Elastic modeling initiative, Part III: 3-D computational modeling, *Soc. Expl. Geophys. Confer. Proceed*. 68:1803–1806.

Levander, A. R. (1988). Fourth-order finite-difference P-SV seismograms, *Geophysics* 53: 1425–1436.

Mayeda, K., and W. Walter (1996). Moment, energy, stress drop, and source spectra of western United States earthquakes from regional coda envelopes, *Jour. Geophys. Res*. 101: 11,195–11,208.

Myers, S.C., W.R. Walter, K. Mayeda, L. Glenn, (1999). Observations in support of Rg scattering as a source for explosion S waves: Regional and local recordings of the 1997 Kazakhstan depth of burial experiment, *Bull. Seismol. Soc. Am*. 89: 544–549.

Myers, S. C., D. B. Harris, M. L. Anderson, W. L. Rodi, W. R. Walter, M. P. Flanagan, and Flori Ryall (2003). Relative location accuracy and waveform subspace detector, in *Proceedings of the 25th Seismic Research Review—Nuclear Explosion Monitoring: Building the Knowledge Base*, LA-UR-03-6029, Vol. 1, pp. 259–268.

Mooney, W., G. Laske, G. Masters (1998). Crust 5.1: a global crustal model at 5x5 degrees, *Jour. Geophys. Res*. 103: 727–747.

Nuttli, O.W. (1986). Yield estimates of Nevada Test Site explosions obtained from seismic Lg waves, *J. Geophys. Res*. 91: 2137–2151.

Patton, H.J., and S.R. Taylor (1984). Q-structure of the basin and range from surface waves, *Jour. Geophys. Res*. 89: (NB8): 6929–6940.

Patton, H.J. (2001). Regional magnitude scaling, tranportability, and Ms:mb discrimination at small magnitudes, *Pageoph* 158: 1951–2015.

Pomeroy, P., W. Best, and T. McEvilly (1982). Test ban treaty verification with regional data – a review, *Bull. Seismol. Soc. Am*. 72: S89–S129.

Preston, L., K. Smith, and D. vonSeggern (2005). 3D velocity structure of the Yucca Mountain, *Seismo. Soc. Am. Spring Meeting, Presented at the 2005 SSA meeting*, Incline, NV.

Sweeney, J.J., S.C. Myers, and J.L. Wagoner (2006). Automated development of 3D local traveltime models, in *Proceedings of the 28th Seismic Research Review: Ground-Based Nuclear Explosion Monitoring Technologies*, LA-UR-06-5471, Vol. 1, pp. 530–537.

Vogfjord, K. (1997). Effect of explosion depth and earth structure on the excitation of Lg waves: S* revisited, *Bull. Seismol. Soc. Am*. 87: 1100–1114.

Wallace, T., D. Helmberger, and G. Engen (1985). Evidence for tectonic release from underground nuclear explosions in long period S waves, *Bull. Seismol. Soc. Am*. 75: 157–174.

Walter, W., K, Mayeda, and H. Patton (1995). Phase and spectral ratio discrimination between NTS earthquakes and explosions: Part I: empirical observations, *Bull. Seismol. Soc. Am*. 85: 1050–1067.

Zandt, G., S. C Myers, T. C Wallace (1995). Curst and mantle structure across the Basin and Range – Colorado plateau at 37° north latitude and implications for Cenozoic extension mechanism, *Jour. Geophys. Res*. 100: 10,592–10,548.